



The four varieties of South Asian monsoon low-pressure systems and their modulation by tropical intraseasonal variability

Article

Published Version

Creative Commons: Attribution 4.0 (CC-BY)

Open Access

Deoras, A., Hunt, K. ORCID: <https://orcid.org/0000-0003-1480-3755> and Turner, A. ORCID: <https://orcid.org/0000-0002-0642-6876> (2021) The four varieties of South Asian monsoon low-pressure systems and their modulation by tropical intraseasonal variability. *Weather*, 76 (6). pp. 194-200. ISSN 0043-1656 doi: <https://doi.org/10.1002/wea.3997> Available at <https://centaur.reading.ac.uk/97403/>

It is advisable to refer to the publisher's version if you intend to cite from the work. See [Guidance on citing](#).

To link to this article DOI: <http://dx.doi.org/10.1002/wea.3997>

Publisher: Wiley

All outputs in CentAUR are protected by Intellectual Property Rights law, including copyright law. Copyright and IPR is retained by the creators or other copyright holders. Terms and conditions for use of this material are defined in the [End User Agreement](#).

www.reading.ac.uk/centaur

CentAUR

Central Archive at the University of Reading

Reading's research outputs online

The four regional varieties of South Asian monsoon low-pressure systems and their modulation by tropical intraseasonal variability

Akshay Deoras¹,
Kieran M. R. Hunt^{1,2} and
Andrew G. Turner^{1,2}

¹Department of Meteorology, University of Reading, Reading, UK

²National Centre for Atmospheric Science, University of Reading, Reading, UK

Introduction

The Indian subcontinent is affected by synoptic-scale cyclonic vortices each summer monsoon season (June–September). These vortices, known as monsoon low-pressure systems (LPSs), most frequently develop over the head of the Bay of Bengal (BoB) and adjoining land area, propagate west-northwestward over India, and produce abundant precipitation along their tracks (e.g. Mooley, 1973; Godbole, 1977). LPSs have triggered several catastrophic floods in the Indian subcontinent, including the 2018 Kerala floods (Hunt and Menon, 2020). Previous studies have suggested that LPSs, which have an average lifespan of 3 to 5 days, are responsible for around half of the summer monsoon rainfall over India (e.g. Yoon and Chen, 2005; Hunt and Fletcher, 2019).

According to the India Meteorological Department,¹ systems featuring two closed isobars in surface pressure at 2hPa intervals over land, or those featuring 3-minute maximum sustained surface wind speeds of 8.5–13.5 m s⁻¹ over sea are referred to as monsoon depressions, whereas systems weaker than this are referred to as monsoon low-pressure areas. Typically, around 14 LPSs form each summer and half of them intensify into monsoon depressions (Boos *et al.*, 2015). Both the frequency and lifespan of LPSs are larger in July and August than in June and September (Krishnamurthy and Ajayamohan, 2010).

Of particular importance to this study are the structures of thermodynamic and moisture fields of LPSs (Godbole, 1977; Hunt *et al.*, 2016) and the relationship between intraseasonal modes of rainfall and LPS frequency

(Krishnamurthy and Ajayamohan, 2010). LPSs have a warm-over-cold core structure; the lower-tropospheric cold core is a result of evaporative cooling of precipitation and reduced insolation due to significant cloud cover (Sarker and Choudhary, 1988; Sørland and Sorteberg, 2015), whereas latent heating from deep convection is responsible for the warm core (Keshavamurthy *et al.*, 1978). The LPS frequency during the active phase of the monsoon is nearly 3.5 times higher than during the break phase, and nearly 7 times higher for monsoon depressions (Goswami *et al.*, 2003; Krishnamurthy and Shukla, 2007). Krishnamurthy and Ajayamohan (2010) analysed LPSs during all phases of the two intraseasonal modes, which were first obtained by Krishnamurthy and Shukla (2007, 2008). These intraseasonal modes are related to the Boreal Summer Intraseasonal Oscillation (BSISO), to be discussed later in this section. They concluded that the location and area covered by LPSs are tied to the propagation of convective anomalies of these intraseasonal modes — LPS tracks occur further south over the subcontinent when convective anomalies are located over the equatorial Indian Ocean, and further north when the convective anomalies are located over India and the northwestern Pacific Ocean.

Haertel and Boos (2017) found that LPS frequency is not significantly affected by the amplitude of the Madden-Julian Oscillation (MJO). With increasing MJO amplitude, there is a slight decrease in the number of monsoon low-pressure areas, but roughly the same number of monsoon depressions and deep depressions. However, LPS frequency is modulated by MJO phase, with phases 4–6 (where convection is favoured over the eastern Indian Ocean and the western Pacific Ocean) supporting the genesis of LPSs in general. While the eastward-propagating MJO is the most prominent mode of the tropical intraseasonal oscillation (ISO) in boreal winter, the BSISO prevails in boreal summer (Wang and Xie, 1997; Kikuchi *et al.*, 2012). The convective anomalies associated with the BSISO show an additional northward/northeastward propagation over the Indian summer monsoon region

(e.g. Yasunari, 1979) and northward/northwestward propagation over the Western North Pacific and East Asian regions (e.g. Murakami, 1984). Suhas *et al.* (2013) proposed the Monsoon Intraseasonal Oscillation (MISO) index as another index for monitoring the northward-propagating component of the ISO over the Indian summer monsoon region. Unlike for the MJO, formal relationships between LPS frequency and the northward-propagating component of the ISO, as measured by the BSISO and MISO indices, have not been explored in the past.

Hunt and Fletcher (2019) identified four regional varieties of LPSs by applying a feature-tracking algorithm to ERA-Interim reanalysis and then using a *k*-means technique (MacQueen, 1967) to cluster the resulting tracks. LPSs forming over the head of the Bay of Bengal and nearby coastal regions were named BoB-short or BoB-long depending on the track length. They found that BoB-short LPSs are confined to eastern India, unlike BoB-long LPSs that propagate across the peninsula, reaching western and northwestern parts of India. The other two LPS varieties (Arabian and Sri Lankan) were situated over the Arabian Sea and Sri Lanka, respectively. As LPS studies are typically focused on monsoon depressions, Arabian and Sri Lankan LPSs have not received much attention. Moreover, the detailed behaviour of four LPS varieties during all phases of the ISO has not been examined. In this study, we aim to understand the following aspects:

1. What are the differences between track statistics for the four LPS varieties?
2. Are there important structural or thermodynamical differences between the different LPS varieties?
3. How much precipitation is contributed by each LPS variety to the seasonal mean precipitation?
4. How does the ISO, as measured by the BSISO, MISO and MJO indices, modulate LPS activity of each variety?

Data and methods

ERA-Interim

We use the European Centre for Medium-Range Weather Forecasts ERA-Interim (ERA-

¹http://imd.nagpur.gov.in/docs_general/monsoonfaq.pdf

l) reanalysis dataset (Dee *et al.*, 2011) to analyse vertical structures of LPSs. ERA-I is available from January 1979 to August 2019 at a spatial resolution of $\sim 0.7^\circ \times 0.7^\circ$ and a temporal resolution of 6 hours. For vertical composites, we use 27 output pressure levels from 1000 to 100hPa.

LPS catalogue

We use an extended version of an LPS catalogue that was initially created by Hunt and Fletcher (2019)². In this catalogue, LPSs, which include monsoon low-pressure areas, depressions and deep depressions, are tracked in ERA-I. We retain those LPSs which had their genesis during June–September 1979–2018 as ERA-I data for September 2019 are not available.

Tropical Rainfall Measuring Mission

Version 7 of the Tropical Rainfall Measuring Mission 3B42 product (Huffman *et al.*, 2007) is used to calculate the precipitation contribution of LPSs. The dataset is available from 1998 to 2019 at a three-hourly temporal resolution on a 0.25° grid.

Indices

The MJO indices (Wheeler and Hendon, 2004) were obtained from the Bureau of Meteorology, Australia³.

The MISO indices (Suhas *et al.*, 2013) were downloaded from the Indian Institute of Tropical Meteorology, Pune⁴. The BSISO indices (Kikuchi and Wang, 2010; Kikuchi *et al.*, 2012; Kikuchi, 2020) were obtained from the International Pacific Research Center.⁵ Each index has a daily temporal resolution, and it is separated into eight phases that represent different geographical locations (e.g. phases 2–3 of the MJO

index represent the Indian Ocean, whereas phases 2–3 of the BSISO and MISO indices represent the Indian Ocean–East Asia region and central India respectively). The three indices are computed from different fields and over different regions – outgoing long-wave radiation (OLR) and zonal wind anomalies (averaged over 15°S – 15°N) at 850 and 200 hPa are considered for the MJO; OLR and zonal wind at 850 hPa (over 10°S – 40°N , 40°E – 160°E) are considered for the BSISO; and daily rainfall data (over 12.5°S – 30.5°N , 60.5°E – 95.5°E) is considered for the MISO. The MJO index is computed for all months, whereas the BSISO index is computed for May to October and the MISO index is computed for June to September. From the common period of June to September 1998–2018, only those dates on which an index exceeds one standard deviation have been considered, in order to clearly identify the phase at a given instant. There are: 4, 5 and 7 Arabian LPSs; 47, 49 and 47 BoB-short LPSs; 22, 21 and 31 BoB-long LPSs; and 25, 26 and 23 Sri Lankan LPSs for which the amplitude of the BSISO, MISO and MJO respectively is less than one. We refer to such LPSs as belonging to phase zero, for ease.

Significance testing

We perform the independent *t*-test (Snedecor and Cochran, 1989) to determine if the vertical composite of an LPS variety is significantly different from the all-LPS composite. Our null hypothesis states that an LPS variety and the all-LPS composite have identical average values. Thus, areas where a 95% significance level is not satisfied are coloured grey in the figure.

Track statistics

Frequency and track characteristics

During June–September 1979–2018, 22 Arabian, 229 BoB-short, 135 BoB-long and 119 Sri Lankan LPSs are identified. Table 1 shows the statistics for these four LPS varieties. BoB-short LPSs have the largest frequency of $5.7 (\pm 1.7)$ systems per season, whereas Arabian LPSs have the smallest frequency of $0.6 (\pm 0.8)$ systems per sea-

son. The figures in brackets indicate one standard deviation. The interannual correlation coefficient between BoB-short and BoB-long LPSs is -0.49 , suggesting that conditions that benefit one may suppress the other.

All LPS varieties can form throughout the summer monsoon season; the frequency of BoB-short as well as BoB-long LPSs is larger in July and August than in June and September, in agreement with Krishnamurthy and Ajayamohan (2010). The frequency of Arabian LPSs is the largest in June. In our analysis period, there are 13 LPSs in June, of which 8 formed during 1–7 June, which is the typical monsoon onset period over Kerala. This suggests that these LPSs are related to the monsoon onset vortex. The conditions over the Arabian Sea for LPS genesis are more favourable in June than in other months. The position of the Somali jet is further towards the equator in June than in other months of the summer monsoon season. As there is positive low-level vorticity poleward and negative low-level vorticity equatorward of the jet axis, the positive low-level vorticity over the genesis region reaches a maximum value in June, supporting the genesis of Arabian LPSs (Evan and Camargo, 2011). In contrast, Sri Lankan LPSs are least common in June, but most common in July.

BoB-long and BoB-short LPSs have mean durations of 7.6 and 7.3 days respectively, which are larger than those of Arabian and Sri Lankan LPSs. The mean track length and mean intensity (850 hPa relative vorticity at the system centre) of BoB-long LPSs are the largest among all LPS varieties. Arabian LPSs have the fastest mean propagation speed of 2.5 ms^{-1} ; whereas BoB-short as well as Sri Lankan LPSs have the slowest mean propagation speed of 1.5 ms^{-1} .

Track density

Figure 1 shows the track density of each regional variety during June–September 1979–2018. The track density is calculated by a kernel density estimation (KDE) technique (Bowman and Azzalini, 1997). The KDE is a non-parametric technique to construct

²Available at http://gws-access.jasmin.ac.uk/public/incompass/kieran/track_data/lps-tracks_v2.1.2_1979-2019.csv

³<http://www.bom.gov.au/climate/mjo/graphics/rmm.74toRealtime.txt>

⁴https://www.tropmet.res.in/erpas/files/miso_data.php

⁵http://iprc.soest.hawaii.edu/users/kazuyoshi/ISO_index/data/BSISO_25-90bpfil_pc.txt

Table 1

The statistics for four regional varieties of South Asian monsoon low-pressure systems during June–September 1979–2018. Figures in brackets indicate the population standard deviation from the mean. The mean 850hPa relative vorticity is taken from the centre of systems.

Variety	Number per season (June–September)	Mean track duration (days)	Mean track length (km)	Mean propagation speed (ms^{-1})	Mean 850hPa relative vorticity (10^{-5}s^{-1})
Arabian	0.6 (0.8)	6.1	1105	2.5	5.3
BoB-long	3.4 (1.6)	7.6	1370	2.4	5.8
BoB-short	5.7 (1.7)	7.3	796	1.5	5.0
Sri Lankan	3.0 (1.4)	5.0	629	1.5	3.3

a smooth probability density estimate of observed data, and it has been used to calculate the track density of tropical cyclones over the north Indian Ocean (e.g. Wahiduzzaman and Yeasmin, 2019). The track density of BoB LPSs is maximised over eastern India, where there are about eight LPSs per square degree for the 40-year period. The peak track density of Sri Lankan LPSs is similar in magnitude to that of BoB-long LPSs. In contrast, Arabian LPSs have the smallest peak track density of 0.1–0.2 LPSs per square degree for the 40-year period.

Vertical structure of temperature and moisture

Figure 2 shows the composite vertical structures of temperature anomalies and equivalent potential temperature anomalies for each regional LPS variety. As LPS frequency shows significant variability on the monthly timescale, we consider a monthly climatology instead of a seasonal climatology. We first compute a climatology for each month during June–September 1979–2018, and then calculate anomalies against the climatology of the respective month. For compos-

ing, LPSs of each variety are centred on 0° relative latitude and 0° relative longitude at each time step. The vertical structure is then drawn above the zero-latitude line in a horizontal composite, similar to the method followed by Hunt *et al.* (2016). Thus, relative west is to the left and relative east is to the right of 0° relative longitude.

The expected warm-over-cold core structure is seen in each variety; the magnitude of the warm core is the largest in Arabian LPSs (Figure 2a), implying maximum latent heating and precipitation from deep convection, whereas it is the smallest in Sri Lankan LPSs (Figure 2d). The warm core is located at equal altitude in BoB-long and BoB-short LPSs. However, its magnitude is larger by 0.2 K in BoB-long LPSs than in BoB-short LPSs. In Sri Lankan LPSs, the warm core does not extend into the upper troposphere as evidenced by negative temperature anomalies above 300 hPa.

BoB-long LPSs feature the strongest cold core, which sits at the composite centre and extends up to the 700 hPa level. BoB-short LPSs feature a similar cold-core structure, but the magnitude is smaller than that of BoB-long LPSs. Arabian LPSs feature a weaker cold-core structure; their cold core is elevated, and there are maximum anomalies between 850 and 700 hPa. Similar to the warm core, the magnitude of the cold core of Sri Lankan LPSs is the smallest among all LPS varieties, and the maximum anomaly is located below the 925 hPa level. The weak thermal structure of Sri Lankan LPSs is related to the weak intensity of these systems.

We now investigate equivalent potential temperature (θ_e), which is an important thermodynamic quantity for determining moisture content and stability of an air parcel. Large θ_e anomaly values for LPSs imply strong latent heating from deep convection, which is related to intense LPSs having a large moisture content. The maximum in θ_e is located at a lower altitude than that in the temperature anomalies, suggesting that all four varieties have a maximum moisture content in the lower troposphere. Arabian LPSs feature the largest anomalies of 8 K, while Sri Lankan LPSs feature the smallest anomalies of 2 K. Thus, these results are consistent with the observed intensity of four LPS varieties.

Precipitation contribution

It is crucial to determine the precipitation contribution of each LPS regional variety to the seasonal mean precipitation (June–September) as this information can help in designing forecasting products for hydrological services. This will ultimately help in improving the management of water resources as well as flood forecasting in the Indian subcontinent. Following Hunt and Fletcher (2019), we attribute precipitation to

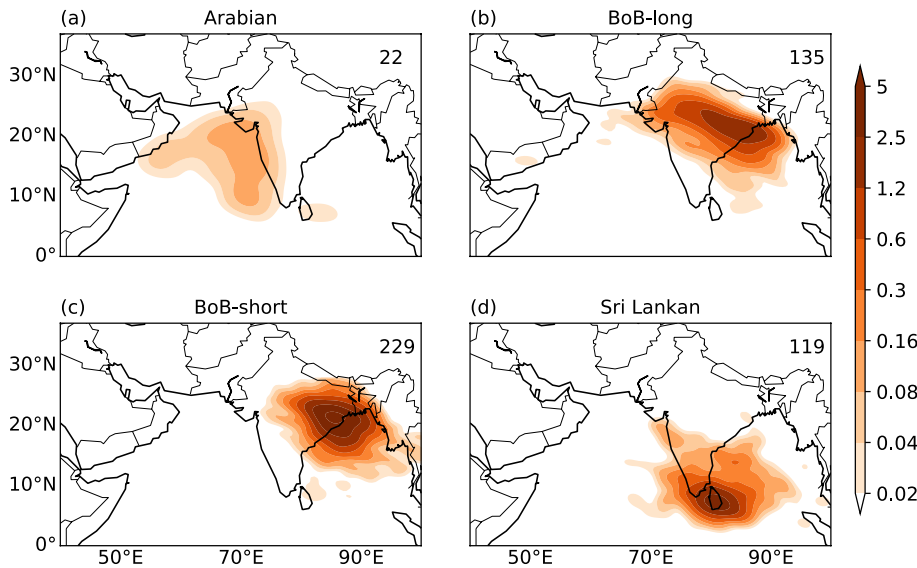


Figure 1. (a–d) The track density of four regional varieties of South Asian monsoon low-pressure systems (LPSs). The track density is calculated using a kernel density estimation technique. The total number of LPSs belonging to each variety is shown in each subplot. The unit of track density is LPS number per square degree for June–September 1979–2018.

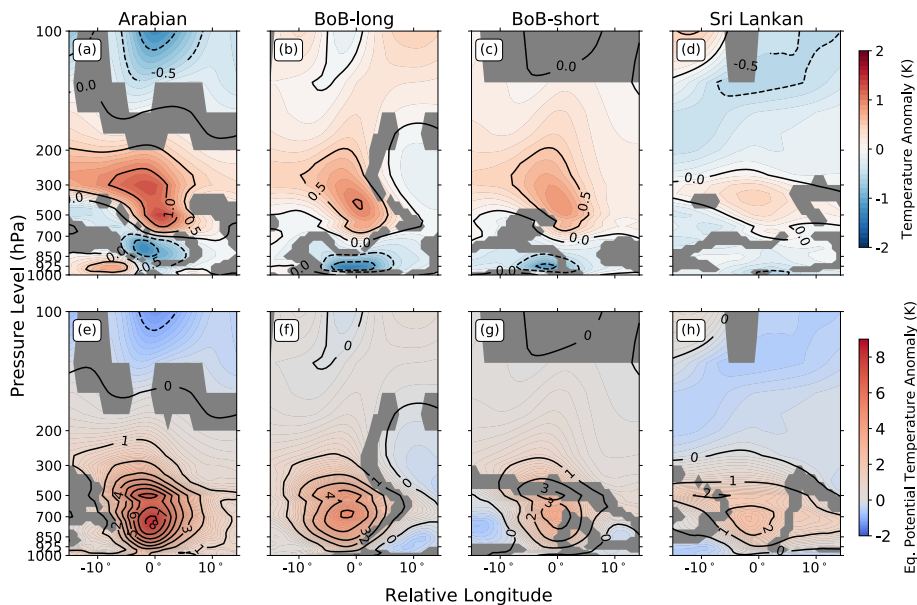


Figure 2. (a–d) Vertical structure of temperature anomalies (K), and (e–h) equivalent potential temperature anomalies (K) for storm-centred composites of four regional varieties of South Asian monsoon low-pressure systems (LPSs) during June–September 1979–2018. Solid contour lines indicate positive anomalies, whereas dashed contour lines indicate negative anomalies. Coloured contours are greyed out where an LPS composite does not significantly differ from the all-LPS composite at the 95% level.

an LPS if it falls within a distance of 800 km from the LPS centre at each time step.

Figure 3 shows the precipitation contribution and the mean track of each LPS variety. BoB-short LPSs have the largest precipitation contribution over the western Bay of Bengal and adjoining eastern India. They cause more than 40% of the seasonal precipitation over this region and 10–30% of the seasonal precipitation over parts of central India, Bhutan, southern Tibet, Nepal, Bangladesh and western Myanmar. BoB-long LPSs also cause rainfall over eastern India, but the attributed rainfall is smaller due to the faster propagation, longer tracks and smaller frequency than those of BoB-short LPSs. We note that 10–30% of the seasonal precipitation over parts of Pakistan and central, western and northwestern parts of India is attributed to BoB-long LPSs. Over southern parts of Afghanistan and adjoining eastern Iran, the attributed precipitation exceeds 40%.

Sri Lankan LPSs are responsible for 20–40% of the seasonal rainfall over Sri Lanka and adjoining parts of southeastern India. In fact, the attributed precipitation exceeds 40% over northern Sri Lanka. In contrast, Arabian LPSs provide a very low precipitation contribution of up to 20% over the central Arabian Sea and less than 10% over the western coast of India and Pakistan. While our results agree with Hunt and Fletcher (2019) in general, we find a larger precipitation contribution from Sri Lankan LPSs and a smaller contribution from Arabian LPSs than their results.

Modulation of LPS activity by the ISO

In this section, we investigate how the ISO modulates the frequency of four regional LPS varieties. As the ISO can be well predicted on the sub-seasonal time scale (e.g. Fu *et al.*, 2007), a better understanding of the ISO-LPS relationship can help in providing useful LPS forecasts with lead times of several weeks, which will benefit weather-dependent socio-economic sectors. Figure 4 shows the anomalous occurrence of four LPS varieties in each phase of the BSISO, MISO and MJO during June–September 1998–2018. The anomalous occurrence is a ratio of the difference between the number of LPSs whose genesis occurs in each phase and the climatological expected value of LPSs in all phases to the climatological expected value of LPSs in all phases. Thus, a 0% value indicates that the frequency of occurrence of LPSs equals the climatological expected value, 100% indicates twice that of the climatological expected value, and –100% indicates no occurrence of LPSs. The location of convective anomalies in a given phase of the MISO is similar to that in the BSISO when there is a phase difference of five (not shown). Hence, MISO phases in Figure 4 have been offset by five phases to align them with the corresponding BSISO phases.

BoB-long and BoB-short LPSs form during all phases of the BSISO, MISO and MJO. However, Arabian LPSs are only found to form during BSISO phases 2–4, MISO phases

1, 3 and 8, and MJO phases 1–3. Sri Lankan LPSs form only during BSISO phases 1–4 and 7–8, MISO phases 1–2 and 4–8, and MJO phases 1–4 and 6–8. Their frequency peaks in BSISO phases 2–3 and MISO phases 7–8. The anomalous frequency of Arabian and Sri Lankan LPSs is maximum in MJO phases 1–2, when convection is over the Indian Ocean and adjoining parts of eastern Africa. BoB systems follow a similar pattern, but their frequency peaks several phases later as the ISO propagates northward. As the frequency of Arabian LPSs is very small, the ISO controls them more strongly than BoB and Sri Lankan LPSs.

We perform a composite analysis of 500 hPa specific humidity, 850 hPa vector wind and 700 hPa vertical velocity for all phases of the BSISO, MISO and MJO to understand the results. These parameters are important for deep convection and genesis of LPSs (e.g. Sikka, 1978). The results are shown in Figures S1–S6, available in the Supporting Information accompanying the online version of this article. Figure S1 shows anomalies of 500 hPa specific humidity and 700 hPa vertical velocity for different phases of the BSISO, whereas Figure S2 shows 850 hPa vector wind anomalies. These anomalies are computed against a summer mean climatology (June–September 1979–2018). In BSISO phase 1, positive specific humidity anomalies and anomalous ascent first appear to the south of Sri Lanka and there is a cyclonic shear over Sri Lanka (Figure S2). In BSISO phases 2–4, these anomalies intensify and propagate northward/northeastward, favouring the genesis of BoB systems. While convection is active over the Bay of Bengal, negative specific humidity anomalies and anomalous descent develop over Sri Lanka and adjoining parts of the Arabian Sea, which suppress LPS frequency. The negative anomalies propagate in a similar manner, suppressing frequency of BoB systems several phases later. We find similar results for the MISO (Figures S3 and S4) and MJO (Figures S5 and S6).

As BoB-short and BoB-long LPSs have similar features and genesis regions, the latter could be considered as an extension of the former. We now understand if the ISO forcing has any role in evolving BoB-short LPSs into BoB-long LPSs. Krishnan *et al.* (2011) investigated long-lived BoB monsoon depressions during 2006. They found that the lifespan of these systems was enhanced due to an increase in barotropic instability of the large-scale monsoon flow, moisture over the Bay of Bengal, and mid-level flows entering the stratiform rain region. They concluded that barotropic instability was enhanced due to an increase in the meridional shear of the zonal wind around 21°N. In this study, in BSISO phases 5–7, MISO phases 2–4 and MJO phases 4–5,

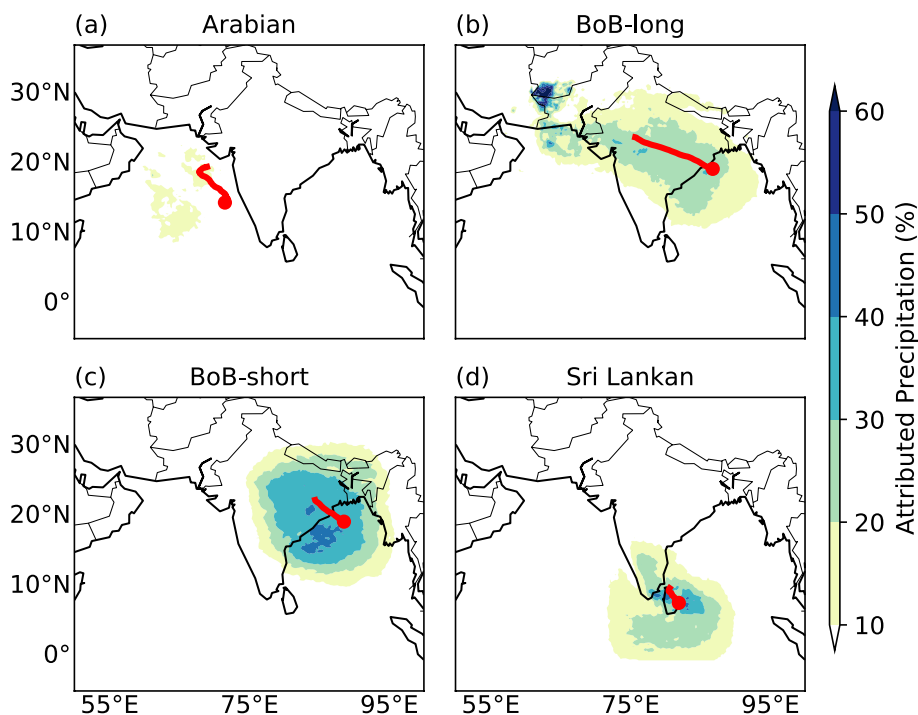


Figure 3. (a–d) Percentage of seasonal (June–September 1998–2018) precipitation attributed to four regional varieties of South Asian monsoon low-pressure systems. A solid red line shows the mean track of each variety, whereas a red dot shows the genesis location. Rainfall is attributed to a system if it falls within 800 km of its centre.

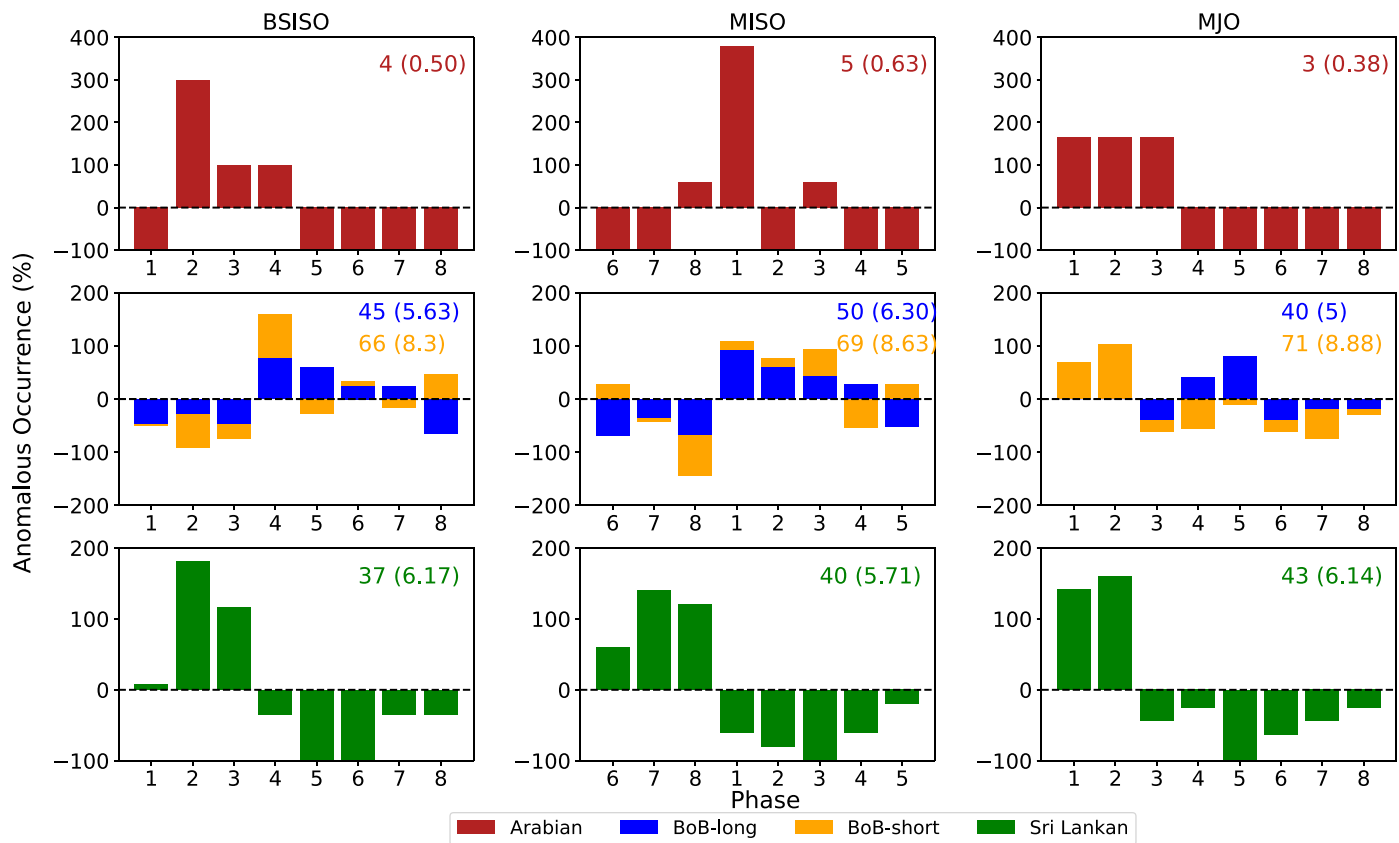


Figure 4. Anomalous occurrence (%) of four regional varieties of South Asian monsoon low-pressure systems (LPSs) during phases of the Boreal Summer Intraseasonal Oscillation (BSISO), Monsoon Intraseasonal Oscillation (MISO) and Madden-Julian Oscillation (MJO) over June–September 1998–2018. Numbers in subfigures indicate the total number of LPSs. A 0% value indicates that the frequency of occurrence of LPSs equals the climatological expected value (shown in brackets in each subfigure), whereas 100% indicates twice that of the climatological mean value. A –100% value indicates no occurrence of LPSs. Only those LPSs occurring during the BSISO, MISO or MJO in which the amplitude exceeds one standard deviation are retained. The MISO phases have been phase-shifted by 5 to align with the corresponding BSISO phases. Bars for BoB-long and BoB-short LPSs are not subdivided — they represent the sum of individual changes to these LPS varieties. Note the different y-axes in subfigures for Arabian, BoB and Sri Lankan LPSs.

which feature most BoB-long LPSs, there is an enhancement of barotropic instability, as evidenced by an increase in the meridional shear of the zonal wind anomalies. Furthermore, there is more mid-tropospheric moisture and anomalous ascent over the monsoon trough region in these phases than those having a smaller frequency of BoB-long LPSs. Therefore, ISO forcing helps in the evolution of BoB-short LPSs into BoB-long LPSs. Further investigations are needed to examine the role of internal dynamics in this process.

Discussion and conclusions

South Asian monsoon low-pressure systems (LPSs) are major rain-bearing synoptic-scale cyclonic vortices. LPSs originating over the head of the Bay of Bengal (BoB) and nearby coastal regions bring around half of the summer monsoon precipitation to India and can trigger catastrophic floods. As several studies have investigated various features of mainly strong LPSs such as Bay of Bengal monsoon depressions, weaker LPSs remain excluded. In this study, we used a catalogue of four regional varieties of LPSs (Hunt and Fletcher, 2019)

that occurred during June–September 1979–2018. Track statistics, thermal and moisture structures, and the precipitation contribution of each variety were examined. The modulation of LPS activity of each variety by the tropical intraseasonal oscillation (ISO) was investigated. The results are summarised as follows.

The differences between track statistics

We identified 22 LPSs over the Arabian Sea and 119 over the Sri Lankan region. In addition, 364 LPSs were identified over the head of the Bay of Bengal and nearby coastal regions, of which 229 LPSs were confined to eastern India (BoB-short) and 135 LPSs travelled to western and northwestern India (BoB-long). LPSs were most common in July and August, except for Arabian LPSs, which were most common in June due to the possible role of monsoon onset conditions. We found that BoB-long LPSs were the strongest and Arabian LPSs were the fastest among all varieties. In contrast, Sri Lankan LPSs were the weakest, and along with BoB-short LPSs, they were the slowest among all LPSs.

Vertical structure

All four LPS varieties featured a warm-over-cold thermal structure, which is commonly seen in LPSs over South Asia (e.g. Hunt *et al.*, 2016). Arabian LPSs featured the strongest warm core, and BoB-long LPSs featured the strongest cold core. In contrast, Sri Lankan LPSs had the weakest warm core and cold core structure, which was related to their weak intensity. All four LPS varieties had their maximum anomaly in equivalent potential temperature in the lower troposphere; Arabian and Sri Lankan LPSs had the largest and smallest anomalies respectively.

Precipitation

We calculated the precipitation contribution of each LPS variety to the summer mean precipitation. We found that BoB-short LPSs had the largest precipitation contribution over the western Bay of Bengal and nearby coastal regions; BoB-long LPSs were the major precipitation contributors to interior parts of India as well as parts of Pakistan, Iran and Afghanistan. In contrast, Arabian LPSs had the smallest precipitation contribution, whereas Sri Lankan LPSs had a

moderate contribution to rainfall over Sri Lanka and adjoining parts of southern India.

Modulation of LPSs by the ISO

We investigated the anomalous occurrence of each LPS variety during June–September 1998–2018 and found that only BoB-short and BoB-long LPSs formed in all phases (amplitude greater than one standard deviation) of the BSISO, MISO and MJO, which are the three commonly used indices for monitoring the ISO. The propagation of the ISO modulated the anomalous occurrence of each variety; the anomalous occurrence of Arabian and Sri Lankan LPSs peaked when the ISO was active over Sri Lanka and adjoining parts of the Arabian Sea, whereas that of BoB systems peaked several phases later with the northward/northeastward propagation of the ISO. We found that cyclonic shear, positive specific humidity anomalies and anomalous ascent favoured LPS genesis, while negative specific humidity anomalies and anomalous descent opposed LPS genesis.

This study opens a new avenue for research on four regional LPS varieties and the role of ISO forcing in modulating their frequency. Further investigation is needed to compare more dynamical properties of the four varieties. In addition, the genesis mechanisms of Sri Lankan LPSs need to be understood. Here we speculate that the interaction between cross-equatorial winds of the monsoon and the high-central Sri Lankan terrain provides low-level cyclonic vorticity on the lee side for spin up of Sri Lankan LPSs.

Acknowledgements

AD is funded through the Scholarship for Higher Education in Foreign Countries programme, an initiative of the Department of Higher and Technical Education, Government of Maharashtra, India. KMRH is supported through the Weather and Climate Science for Service Partnership (WCSSP) India, a collaborative initiative between the Met Office, supported by the UK Government's Newton Fund and the Indian Ministry of Earth Sciences (MoES). AGT acknowledges the INCOMPASS project funded by the Natural Environment Research Council (grant NE/P003117/1). The processed dataset containing tracks and intensities of four regional LPS varieties is available at <https://doi.org/10.5281/zenodo.4572899>.

References

- Boos WR, Hurley JV, Murthy VS.** 2015. Adiabatic westward drift of Indian monsoon depressions. *Q. J. R. Meteorol. Soc.* **141**(689): 1035–1048.
- Bowman AW, Azzalini A.** 1997. *Applied Smoothing Techniques for Data Analysis: The Kernel Approach with S-Plus Illustrations*, Vol. 18. OUP: Oxford, UK.

- Dee DP, Uppala SM, Simmons AJ et al.** 2011. The ERA-Interim reanalysis: configuration and performance of the data assimilation system. *Q. J. R. Meteorol. Soc.* **137**(656): 553–597.
- Evan AT, Camargo SJ.** 2011. A climatology of Arabian Sea cyclonic storms. *J. Clim.* **24**(1): 140–158.
- Fu X, Wang B, Waliser DE et al.** 2007. Impact of atmosphere–ocean coupling on the predictability of monsoon intraseasonal oscillations. *J. Atmos. Sci.* **64**(1): 157–174.
- Godbole RV.** 1977. The composite structure of the monsoon depression. *Tellus* **29**(1): 25–40.
- Goswami BN, Ajayamohan RS, Xavier PK et al.** 2003. Clustering of synoptic activity by Indian summer monsoon intraseasonal oscillations. *Geophys. Res. Lett.* **30**(8): 1431–1434.
- Haertel P, Boos WR.** 2017. Global association of the Madden-Julian Oscillation with monsoon lows and depressions. *Geophys. Res. Lett.* **44**(15): 8065–8074.
- Huffman GJ, Bolvin DT, Nelkin EJ et al.** 2007. The TRMM multisatellite precipitation analysis (TMPA): quasi-global, multiyear, combined-sensor precipitation estimates at fine scales. *J. Hydrometeorol.* **8**(1): 38–55.
- Hunt KMR, Fletcher JK.** 2019. The relationship between Indian monsoon rainfall and low-pressure systems. *Clim. Dyn.* **53**(3–4): 1859–1871.
- Hunt KMR, Menon A.** 2020. The 2018 Kerala floods: a climate change perspective. *Clim. Dyn.* **54**(3): 2433–2446.
- Hunt KMR, Turner AG, Inness PM et al.** 2016. On the structure and dynamics of Indian monsoon depressions. *Mon. Weather Rev.* **144**(9): 3391–3416.
- Keshavamurthy RN, Asnani GC, Pillai PV et al.** 1978. Some studies of the growth of monsoon disturbances. *Proc. Indian Acad. Sci.-Sect. A Earth Planet. Sci.* **87**(3): 61–75.
- Kikuchi K.** 2020. Extension of the bimodal intraseasonal oscillation index using JRA-55 reanalysis. *Clim. Dyn.* **54**(1–2): 919–933.
- Kikuchi K, Wang B.** 2010. Formation of tropical cyclones in the northern Indian Ocean associated with two types of tropical intraseasonal variability modes. *J. Meteorol. Soc. Jpn. Ser. II* **88**(3): 475–496.
- Kikuchi K, Wang B, Kajikawa Y.** 2012. Bimodal representation of the tropical intraseasonal oscillation. *Clim. Dyn.* **38**(9–10): 1989–2000.
- Krishnamurthy V, Ajayamohan RS.** 2010. Composite structure of monsoon low pressure systems and its relation to Indian rainfall. *J. Clim.* **23**(16): 4285–4305.
- Krishnamurthy V, Shukla J.** 2007. Intraseasonal and seasonally persisting patterns of Indian monsoon rainfall. *J. Clim.* **20**(1): 3–20.
- Krishnamurthy V, Shukla J.** 2008. Seasonal persistence and propagation of intraseasonal patterns over the Indian monsoon region. *Clim. Dyn.* **30**(4): 353–369.
- Krishnan R, Ayantika DC, Kumar V et al.** 2011. The long-lived monsoon depressions of 2006 and their linkage with the

Indian Ocean Dipole. *Int. J. Climatol.* **31**(9): 1334–1352.

MacQueen J. 1967. Some methods for classification and analysis of multivariate observations, in *Proceedings of the Fifth Berkeley Symposium on Mathematical Statistics and Probability*, Vol. 1, No. 14, pp. 281–297.

Mooley DA. 1973. Some aspects of Indian monsoon depression and associated rainfall. *Mon. Weather Rev.* **101**: 271–280.

Murakami M. 1984. Analysis of the deep convective activity over the Western Pacific and Southeast Asia. II: seasonal and intraseasonal variations during Northern Summer. *J. Meteorol. Soc. Jpn. Ser. II* **62**(1): 88–108.

Sarker RP, Choudhary A. 1988. A diagnostic study of monsoon depressions. *Mausam* **39**: 9–18.

Sikka DR. 1978. Some aspects of the life history, structure and movement of monsoon depressions, in T. N. Krishnamurti (Ed.), *Monsoon Dynamics*. Birkhäuser: Basel, Switzerland, pp. 1501–1529.

Snedecor GW, Cochran WG. 1989. *Statistical Methods*, 8th Edition. Iowa state University press: Ames, IA.

Sørland SL, Sorteberg A. 2015. The dynamic and thermodynamic structure of monsoon low-pressure systems during extreme rainfall events. *Tellus A* **67**(1): 465–480.

Suhas E, Neena JM, Goswami BN. 2013. An Indian monsoon intraseasonal oscillations (MISO) index for real time monitoring and forecast verification. *Clim. Dyn.* **40**(11–12): 2065–2616.

Wahiduzzaman M, Yeasmin A. 2020. A kernel density estimation approach of North Indian Ocean tropical cyclone formation and the association with convective available potential energy and equivalent potential temperature. *Meteorog. Atmos. Phys.* **132**: 603–612.

Wang B, Xie X. 1997. A model for the boreal summer intraseasonal oscillation. *J. Atmos. Sci.* **54**(1): 72–86.

Wheeler MC, Hendon HH. 2004. An all-season real-time multivariate MJO index: Development of an index for monitoring and prediction. *Mon. Weather Rev.* **132**(8): 1917–1932.

Yasunari T. 1979. Cloudiness fluctuations associated with the Northern Hemisphere summer monsoon. *J. Meteorol. Soc. Jpn. Ser. II* **57**(3): 227–242.

Yoon JH, Chen TC. 2005. Water vapor budget of the Indian monsoon depression. *Tellus A* **57**(5): 770–782.

Correspondence to: A. Deoras
a.s.deoras@pgr.reading.ac.uk

© 2021 The Authors. *Weather* published by John Wiley & Sons Ltd on behalf of the Royal Meteorological Society.

This is an open access article under the terms of the Creative Commons Attribution License, which permits use, distribution and reproduction in any medium, provided the original work is properly cited.

doi: 10.1002/wea.3997

Supporting Information

Figure S1. 500hPa specific humidity anomaly (10^{-3}kgkg^{-1}) in coloured contours and 700hPa vertical velocity anomaly (10^{-2}Pa s^{-1}) in line contours for all phases of the Boreal Summer Intraseasonal Oscillation (BSISO) during June–September 1998–2018. The anomalies are computed against the summer mean climatology (June–September 1979–2018). The vertical velocity anomalies are smoothed using a 2-D Gaussian filter with a smoothing radius of $\sim 200\text{km}$. Solid (dashed) contour lines indicate anomalous

decent (ascent). Coloured and line contours are not shown where the mean surface pressure is less than 500hPa and 700hPa respectively. Phase 0 represents BSISO events featuring an amplitude less than one.

Figure S2. 850hPa vector wind anomalies (ms^{-1}) for all phases of the Boreal Summer Intraseasonal Oscillation (BSISO) during June–September 1998–2018. The anomalies are computed against the summer mean climatology (June–September 1979–2018). Contours are greyed out where the mean surface pressure is less than 850hPa.




Figure S3. As in Figure S1, but for all phases of the Monsoon Intraseasonal Oscillation. Note the different contour interval for 500hPa specific humidity anomaly than shown in Figure S1.

Figure S4. As in Figure S2, but for all phases of the Monsoon Intraseasonal Oscillation.

Figure S5. As in Figure S1, but for all phases of the Madden-Julian Oscillation. Note the different contour interval for 500hPa specific humidity anomaly than shown in Figure S1.

Figure S6. As in Figure S2, but for all phases of the Madden-Julian Oscillation.

First measurements of ocean and atmosphere in the Tropical North Atlantic using *Caravela*, a novel uncrewed surface vessel

Elizabeth Siddle¹ ,
Karen J. Heywood¹ ,
Benjamin G. M. Webber¹ 
and Peter Bromley²

¹Centre for Ocean and Atmospheric Sciences, School of Environmental Sciences, University of East Anglia (UEA), Norwich Research Park, Norwich, UK

²AutoNaut Ltd, Bognor Regis, UK

Introduction

In the tropics, air–sea interactions are an important driver of weather and climate variability and can seed extreme weather events. Robust, accurate and widespread observations at the air–sea interface can improve our understanding of air–sea interaction, help to validate coupled climate models and improve the initial conditions for weather forecasts. A crucial component of the air–sea interaction is the exchange of heat and moisture at the surface. When observing these fluxes, satellites and vessels can only take us so far. To make the next step in understanding air–sea interactions, a comprehensive network of flux measurement platforms, able to sample for extended periods of time, is needed (Cronin *et al.*, 2019).

Nowadays, there are a range of instruments spread across global oceans to capture in situ measurements as part of systems like the Global Ocean Observing System (GOOS) and the EUMETNET Surface Marine Programme. Some examples relevant to the collection of observations at the air–sea interface include the Argo network, moored and drifting buoys, and ships. However, these systems have their limitations: vessels are costly and thus only provide sparse coverage, while moorings rely on deployment and maintenance from a ship, another costly procedure. Argo floats have provided a step change in global coverage of ocean observations, but they typically only surface at 10-day intervals and so are unsuited to studying air–sea interactions on short time scales. Drifting buoys also require deployment by vessel and cannot be targeted to a region of interest, and most drifting platforms only measure near-surface ocean temperature and atmospheric pressure, in addition to recording their position. There are efforts to incorporate a range of meteorological and ocean sensors onto drifters (Centurioni *et al.*, 2019) but their Lagrangian nature still limits their use when a set location is to be studied.

The development of autonomous surface vessels allows targeted measurements of a wide suite of surface ocean and atmospheric

data in particular regions of interest, over long time periods. These vessels will be a key component of future global in situ arrays of observation platforms for air–sea fluxes with high spatial resolution and minimal reliance on ship time. Ideally, these surface vessels would be non-polluting and powered by renewable resources, such as waves, wind and sun.

Autonomous vehicles

The use of autonomous vessels in air–sea interaction studies allows for measurements very close to the water surface, with minimal disturbance to the surrounding air and water parcels. Other advantages include: the ability to launch and recover the vessels from the shore, cutting down costs and reliance on ship time for study; the lack of emissions and low carbon footprint; and the ability to reach previously inaccessible areas. Examples of autonomous vessel deployments to date include Saildrones as part of the SPURS-2 campaign (Zhang *et al.*, 2019), to demonstrate their feasibility as air–sea interaction observational platforms, a wave glider studying air–sea interaction in Drake passage (Thomson and Girton, 2017) and the OCARINA platform developed by Bourras *et al.* (2014), deployed off the west coast of France as part of FROMVAR. It is apparent that the use of surface vehicles in flux deter-